4-2 Development of Two-Way Time and Frequency Transfer System with Dual Pseudo Random Noises

AMAGAI Jun and GOTOH Tadahiro

We developed Two-Way Satellite Time and Frequency Transfer with Dual Pseudo Random Noises as a method to improve precision of measurement. We show theory and implementation of this method.

Keywords
Two-Way Satellite Time and Frequency Transfer (TWSTFT), Binarry Offset Carrier (BOC), Group delay measurement

1 Introduction

Two-Way Satellite Time and Frequency Transfer (TWSTFT) is a method of precisely measuring the difference in the time of 2 clocks that are a far distance apart[1]. Usage of carrier phase and expansion of equivalent bandwidth in group delay measurement can be considered as methods of improving the precision of TWSTFT. Experiments have already been carried out in Europe for use of carrier phase, however this has not yet been made practically useable[2]. For expansion of equivalent bandwidth in group delay measurement simple wider bandwidth methods using high chip rate pseudo random noise[3] have been carried out in Europe and the United States, however this cannot be said to be a practical method when considering operating costs (satellite transponder fees). An effective method for improving precision without increasing operation costs is a method which concentrates power density in the edges of frequency band as with BOC (Binary Offset Carrier[4]) used in global navigation satellite systems[5]. The NICT has developed a method (Two-way time and frequency transfer using dual pseudo random noises: DPN TWSTFT) which uses 2 narrow band pseudo random noises (Dual Pseudo Random Noises: DPN) with separately allocated frequencies and is carrying out verification experiments aimed at practical use[6][7]. This paper introduces the theory for improving the precision of and the implementation methodology for DPN TWSTFT.

2 Theory for precision improvement

The time difference of clocks in 2 distant locations is measured using TWSTFT. Each clock usually outputs a sine-wave signal (Usually 10 MHz or 5 MHz. Hereinafter referred to as the “reference signal”) and a pulse signal per second (Hereinafter referred to as a “1 PPS signal”). The signal generated based on this reference signal and 1 PPS signal is transmitted from each station to the other via a communications satellite and the arrival time of the signal from the remote station is measured using the time of the local station. Taking the difference in arrival times and dividing by 2 we can obtain the difference in times between the 2 stations.

Potential methods for measurement of arrival times include pulse measurement, phase delay measurement of carrier phase and group delay measurement using broadband signals, however group delay measurement using pseudo random noise used in global navigation satellite systems such as GPS allow for measurement of arrival time with ease and relatively high precision and so is widely used in international time comparisons of atomic frequency standard.

In group delay measurement using pseudo random noise, a signal (replica signal) with the same pattern (code) as the measured signal is generated on a processing system and by taking the correlation with the measured signal the group delay can be found as the lag time at the maximum of absolute value of cross-correlation function.

The group delay measurement precision depends on the sharpness of the cross-correlation peak. The width of the cross-correlation peak is in inverse proportion to the signal frequency bandwidth, so the broader the bandwidth, the higher the group delay measurement precision. Below we will examine the group delay in more detail in the frequency domain. Because the group delay is defined as the inclination of the cross spectrum phase, how precisely this inclination can be measured affects the measurement precision. As such, we found that concentrating the signal power on the edges of the band is more effective for improving the delay measurement precision than simply broadening the bandwidth.

In usual TWSTFT a single pseudo random noise is transmitted between each station and group delay is measured reciprocally, however the pseudo random noise signal power is concentrated in the center of the band resulting in a slight degradation in the measurement precision of group delay. In DPN TWSTFT dual pseudo random noises are introduced to improve group delay measurement precision.

Below we will examine the theoretical limits of delay measurement precision for DPN TWSTFT. First we will examine delay measurement precision for the case with single pseudo random noise then, based on this, we will examine delay measurement precision for the case with dual pseudo random noises. Signal processing is usually carried out digitally, so in the following discussion all signals are treated as discrete functions, not continuous functions.

2.1 Delay measurement precision for the case with single pseudo random noise

Consider the correlation between the frequency converted (converted so that the carrier frequency is 0 Hz) pseudo random noise signal with the white noise (Hereinafter referred to as the "received signal") and the replica signal.

Figure 1 shows the pseudo random noise signal with the white noise. Where R_c [bps] is chip rate of the pseudo random noise, $2B$ [Hz] ($-B$ Hz to B Hz) is the band width of the received signal, R_s [bps] ($R_s/2 > B$) is the sampling rate of signal processing.

Figure 2 shows allocation of the complex signal vectors at the frequency f_i [Hz] ($-R_s/2 < f_i < R_s/2$: i denotes each point on the cross spectrum as integers from 1 to N). Where $X(f_i)$ is replica signal component, $Y(f_i)$ is received signal component, Y_n is noise component, $Y'(f_i)$ is the sum of them, and $X(f_i)^* \cdot Y(f_i)$, $X(f_i)^* \cdot Y_n$, $X(f_i)^* \cdot Y'(f_i)$ are cross spectrum components.

Expressing complex numbers X and Y as $|X| e^{i\theta_X}$, $|Y| e^{i\theta_Y}$ using the absolute value and its arguments θ_X, θ_Y, $X^* \cdot Y$ is:

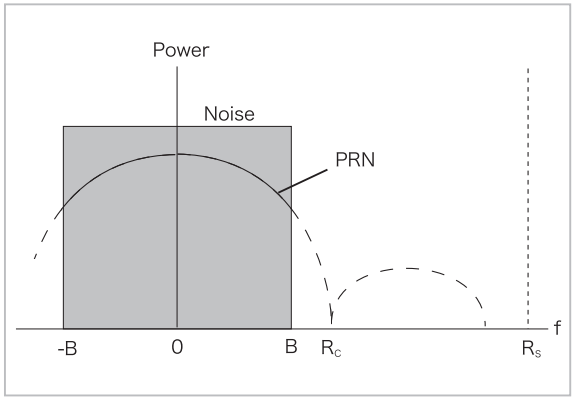

Fig.1 *Pseudo random noise signal with noise*

$$X^* \cdot Y = |X|e^{-i\theta_X} \cdot |Y|e^{i\theta_Y} = |X||Y|e^{i(\theta_Y - \theta_X)} \quad (1)$$

Specifically, the absolute value of $X^* \cdot Y$ is a product of absolute values of X, Y and the argument of $X^* \cdot Y$ is the argument of Y after rotating by argument of X to the right. Hence, each vector of cross spectrum is obtained by multiplying the complex signal vector of each received signal by the replica signal amplitude (Generally 1 or less when normalized) and then rotating by argument of the replica signal to the right, and the relationship between the received signal vector and noise vector is similarly kept even in the cross spectrum.

If the absolute value of Y_n is small, phase error ε is approximately expressed as

$$\varepsilon \approx \frac{Y_n \cdot i_Y}{|Y(f_i)|} \quad (2)$$

where i_Y is the unit vector perpendicular to $Y(f_i)$. $Y_n \cdot i_Y$ is the component of Y_n perpendicular to $Y(f_i)$. The variance of components of the Y_n perpendicular to $Y(f_i)$ is the same as the variance of real or imaginary part of Y_n. Since the number of independent samples for each cross spectrum point is R_sT/N, the variance of $Y_n \cdot i_Y$ is as follows:

$$\overline{(Y_n \cdot i_Y)^2} = \frac{p_n \Delta f N}{2R_s T} \quad (3)$$

where p_n [W/ Hz] is noise power density (constant within range of $-B < f_i < B$, and 0 outside of that range), $\Delta f\,(= R_s/N)$ is the bandwidth of each cross spectrum point, and T is integration time. In addition $|Y(f_i)|$ is expressed as,

$$|Y(f_i)| = \sqrt{p_s(f_i)\Delta f} \quad (4)$$

where $p_s(f_i)$ [W/Hz] is the power density of the received signal at the frequency f_i. So the variance of cross spectrum phase ϕ_i at the frequency f_i can be calculated using the following formula.

$$\sigma_{\phi_i}^2 = \sigma_\varepsilon^2 \approx \frac{\overline{(Y_n \cdot i_Y)^2}}{|Y(f_i)|^2} = \frac{p_n N}{2R_s T p_s(f_i)} \quad (5)$$

Since $p_s(f)$ is proportional to $(\frac{\sin(\pi f/R_c)}{\pi f/R_c})^2$ in the case of BPSK modulation of pseudo random noise with chip rate R_c [bps] (Fig. 3)[3], $p_s(f_i)/p_n$ is

$$\frac{p_s(f_i)}{p_n} = P_s(\frac{\sin(\pi f_i/R_c)}{\pi f_i/R_c})^2 \quad : \quad |f_i| \le B \quad (6)$$

where P_s is ratio of received signal power density and noise power density at the band center (near 0 Hz).

Using $\sigma_{\phi i}$, the delay determination error σ_τ[s] and phase determination error $\sigma_{\phi 0}$[rad] can be obtained as follows[8][9]

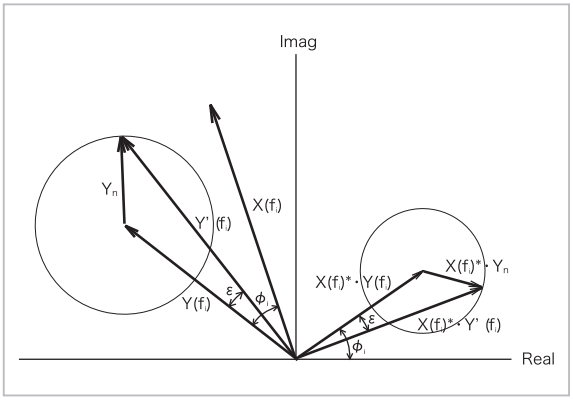

Fig.2 Complex signal vector allocation

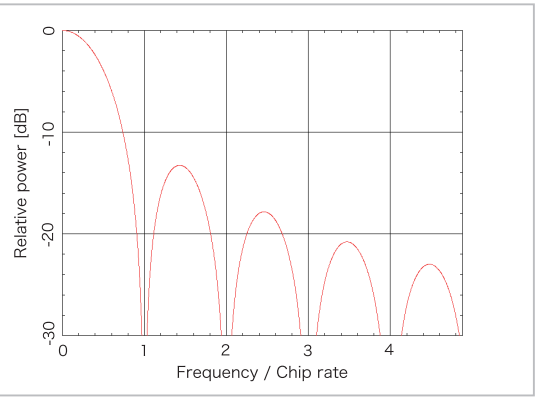

Fig.3 Power spectrum of pseudo random noise

$$\sigma_\tau^2 = \frac{1}{4\pi^2} \frac{\sum_{i=1}^{N} \frac{1}{\sigma_{\phi_i}^2}}{(\sum_{i=1}^{N} \frac{1}{\sigma_{\phi_i}^2})(\sum_{i=1}^{N} \frac{f_i^2}{\sigma_{\phi_i}^2}) - (\sum_{i=1}^{N} \frac{f_i}{\sigma_{\phi_i}^2})^2} \quad (7)$$

$$\sigma_{\phi 0}^2 = \frac{\sum_{i=1}^{N} \frac{f_i{}^2}{\sigma_{\phi_i}^2}}{(\sum_{i=1}^{N} \frac{1}{\sigma_{\phi_i}^2})(\sum_{i=1}^{N} \frac{f_i^2}{\sigma_{\phi_i}^2}) - (\sum_{i=1}^{N} \frac{f_i}{\sigma_{\phi_i}^2})^2} \quad (8)$$

Taking account of $\sum_{i=1}^{N} \frac{f_i}{\sigma_{\phi_i}^2} = 0$ which is derived from the fact that $\sigma_{\phi i}{}^2$ is an even function, by reallocating the cross spectrum points as i=1 at 0 Hz and i=N_B at B Hz, Equation (7) and Equation (8) becomes

$$\sigma_\tau^2 = \frac{1}{8\pi^2 \sum_{i=1}^{N_B} \frac{f_i^2}{\sigma_{\phi_i}^2}} \quad (9)$$

$$\sigma_{\phi 0}^2 = \frac{1}{2 \sum_{i=1}^{N_B} \frac{1}{\sigma_{\phi_i}^2}} \quad (10)$$

Substituting Equation (5) and Equation (6) into Equation (9) and Equation (10) gives

$$\sigma_\tau^2 = \frac{1}{16\pi^2 R_s T \frac{1}{N} P_s \sum_{i=1}^{N_B} f_i^2 (\frac{\sin(\pi f_i/R_c)}{\pi f_i/R_c})^2} \quad (11)$$

$$\sigma_{\phi 0}^2 = \frac{1}{4 R_s T \frac{1}{N} P_s \sum_{i=1}^{N_B} (\frac{\sin(\pi f_i/R_c)}{\pi f_i/R_c})^2} \quad (12)$$

Figures 4 and 5 show bandwidth dependency of measurement precision under the conditions of R_c=1 MHz and C/N_0=57 dBHz for group delay and phase respectively. As shown in Fig. 3, the power density for the portion of the frequency which exceeds $2R_c$ is low compared to that of the center portion, and seems not to contribute to delay measurement precision, however as shown in Fig. 4, the wider the bandwidth, the more improved delay measurement precision is. On the other hand, it is shown in Fig. 5 that the phase measurement precision is not improved even if the bandwidth is increased more than the chip rate.

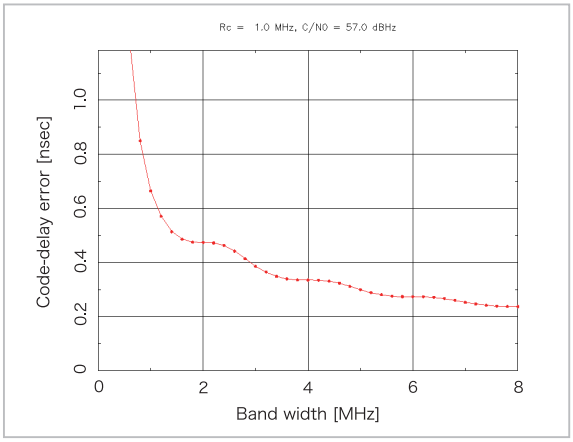

Fig.4 *Bandwidth dependency of delay measurement precision*

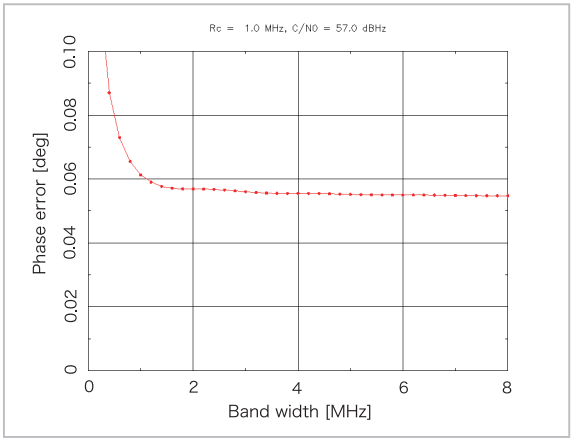

Fig.5 *Bandwidth dependency of phase measurement precision*

2.2 In the case that chip rate equals to a half of the bandwidth

In a special case where the R_c (chip rate) equals to B (a half of the bandwidth), since $\frac{N_B}{N} R_s = R_c$, σ_τ^2 and $\sigma_{\phi 0}^2$ can be expressed as

$$\sigma_\tau^2 = \frac{1}{16 T R_c^3 P_s \frac{1}{N_B} \sum_{i=1}^{N_B} \sin^2(\pi f_i/R_c)} \quad (13)$$

$$\sigma_{\phi 0}^2 = \frac{1}{4 R_c T P_s \frac{1}{N_B} \sum_{i=1}^{N_B} (\frac{\sin(\pi f_i/R_c)}{\pi f_i/R_c})^2} \quad (14)$$

When N_B is sufficiently large,

$$\frac{1}{N_B}\sum_{i=1}^{N_B}\sin^2(\pi f_i/R_c) \approx \frac{1}{2} \tag{15}$$

$$\frac{1}{N_B}\sum_{i=1}^{N_B}\left(\frac{\sin(\pi f_i/R_c)}{\pi f_i/R_c}\right)^2 \approx 0.45 \tag{16}$$

Substituting them into Equations (13) and (14), we obtain

$$\sigma_\tau^2 \approx \frac{1}{8TR_c^3P_s} \tag{17}$$

$$\sigma_{\phi_0}^2 \approx \frac{1}{1.8TR_cP_s} \tag{18}$$

Using Equation (16) C/N_0 is expressed as

$$\begin{aligned} C/N_0 &= 2R_c \times \frac{1}{2N_B} 2P_s \sum_{i=1}^{N_B}\left(\frac{\sin(\pi f_i/R_c)}{\pi f_i/R_c}\right)^2 \\ &\approx 0.9R_cP_s \end{aligned} \tag{19}$$

Therefore, σ_τ and $\sigma_{\phi 0}$ become

$$\sigma_\tau \approx \frac{1}{3R_c\sqrt{TC/N_0}} \tag{20}$$

$$\sigma_{\phi_0} \approx \frac{1}{\sqrt{2TC/N_0}} \tag{21}$$

2.3 Delay measurement precision for the case with Dual Pseudo Random Noises

In this section we discuss delay determination precision for the case of delay measurement using two pseudo random noises separately allocated on the frequency axis.

Consider that pseudo random noise with the chip rate R_c is allocated with frequency separation of $2F_1$ and each pseudo random noise is extracted by a filter with bandwidth of $2R_c$ (correspond to BOC (F_1, R_c)[4]) as shown in Fig. 6. Since group delay is defined as an inclination of the cross spectrum phase, the cross spectrum phases of two PRN's should be on a line as shown in Fig. 6.

Now, divide each filter pass band into $2N_B$ equal slots, and number all slots in two bands from i=1 to i=4N_B in order from lowest frequency. Let the center frequency, the cross spectrum phase and its error for i-th slot be f_i [Hz], ϕ_i [rad] and $\sigma_{\phi i}$ [rad], respectively.

Using $\sigma_{\phi i}$, delay determination error σ_τ[s] can be obtained by[8][9]

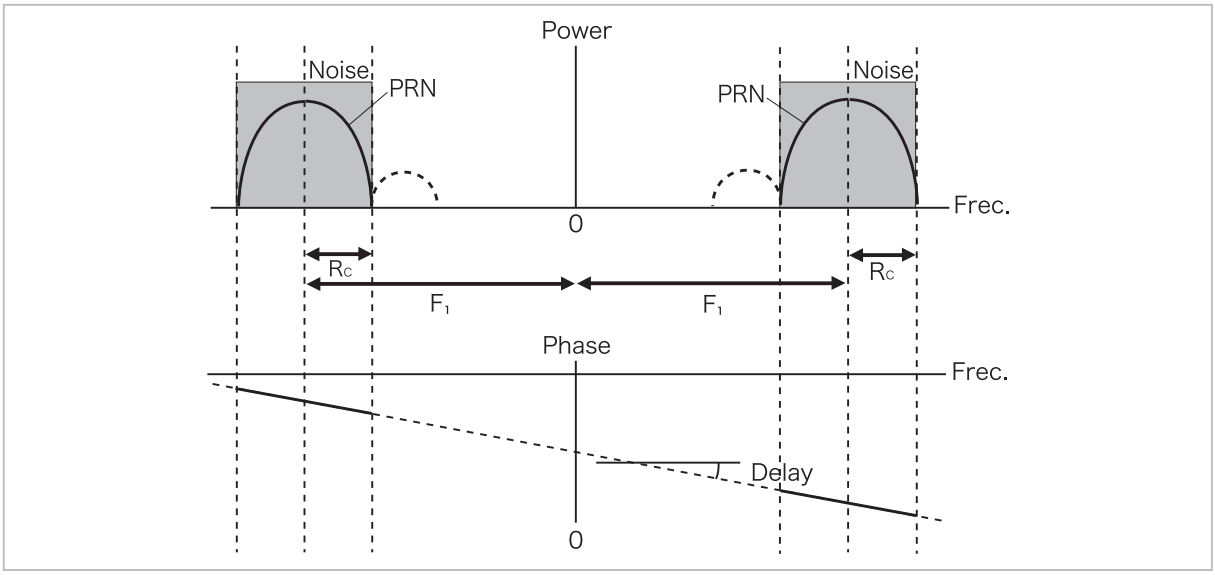

Fig.6 *DPN signal with noise*

Power (Top) and Phase (Bottom) of Cross Spectrum

$$\sigma_\tau^2 = \frac{1}{4\pi^2} \frac{\sum_{i=1}^{4N_B} \frac{1}{\sigma_{\phi_i}^2}}{(\sum_{i=1}^{4N_B} \frac{1}{\sigma_{\phi_i}^2})(\sum_{i=1}^{4N_B} \frac{f_i^2}{\sigma_{\phi_i}^2}) - (\sum_{i=1}^{4N_B} \frac{f_i}{\sigma_{\phi_i}^2})^2} \quad (22)$$

Since $\sigma_{\phi i}{}^2$ is an even function, $\sum_{i=1}^{4N_B} \frac{f_i}{\sigma_{\phi_i}^2} = 0$. In addition, if $F_1 \gg R_c$, then $f_i \fallingdotseq F_1$. Further, taking into account the symmetricity of each pseudo random noise, Equation (22) becomes

$$\sigma_\tau^2 = \frac{1}{8\pi^2 F_1^2 \times 2 \sum_{i=1}^{N_B} \frac{1}{\sigma_{\phi_i}^2}} \quad (23)$$

As mentioned in **2.2**, $1/(2\sum_{i=1}^{N_B} \frac{1}{\sigma_{\phi_i}^2})$ is variance of phase $\sigma_{\phi 0}{}^2$ estimated using single pseudo random noise,

$$\sigma_{\phi_0}^2 \approx \frac{1}{2T\,C/N_0} \quad (24)$$

where T is integration time and C/N_0 is carrier to noise ratio of single pseudo random noise. Therefore, from Equation (23)

$$\sigma_\tau \approx \frac{1}{4\pi F_1 \sqrt{T\,C/N_0}} \quad (25)$$

However, practically, the phases reflecting the group delay determined from each pseudo random noise should be on a line, so the group delay error $\sigma_{\tau s}$ determined from one of the pseudo random noises must satisfy $2\pi(2F_1)\sigma_{\tau s} < \pi$. As mentioned in **2.2**, $\sigma_{\tau s}$ is

$$\sigma_{\tau_s} \approx \frac{1}{3R_c \sqrt{T\,C/N_0}} \quad (26)$$

so,

$$R_c > \frac{4F_1}{3\sqrt{T\,C/N_0}} \quad (27)$$

is the necessary condition for realizing the determination of group delay using multiple pseudo random noise signals. In practically, this is the condition for success for the determination of phase ambiguity at a probability of 1σ, so in order to achieve a stable solution, it is necessary to expand the R_c to several times the right side of Equation (27).

2.4 Restrictions resulting from S/N ratio

Because pseudo random noise is a discrete signal, measured group delay is systematically affected in case of high S/N ratio. For this reason, it is necessary to make the S/N ratio smaller than 1. Now, if the signal power is set to half the noise power it results in

$$\frac{1}{2N_B} 2P_s \sum_{i=1}^{N_B} \left(\frac{\sin(\pi f_i/R_c)}{\pi f_i/R_c}\right)^2 = \frac{1}{2} \quad (28)$$

so from Equation (19)

$$C/N_0 = R_c \quad (29)$$

Therefore the delay measurement precision obtained from DPN is restricted as follows from Equation (25),

$$\sigma_\tau \approx \frac{1}{4\pi F_1 \sqrt{T\,R_c}} \quad (30)$$

and the group delay determination criteria is as follows from Equation (27):

$$R_c^3 > \frac{16F_1^2}{9T} \quad (31)$$

3 Realization methods

In this section we discuss how to realize practical system based on the conditions for delay measurement precision and frequency allocation of DPN TWSTFT discussed in **2**.

3.1 System configuration

The system configuration and the specifications for the conventional TWSTFT are shown in Fig. 7 and Table 1, respectively. Taking account of economical efficiency, ability to spread into a community, and future evolvabil-

ity, it is preferable to reuse currently used equipment as much as possible, and to adopt software processing on a personal computer instead of equipping hardware with high performance function.

The bandwidth of transponders equipped on ordinary geostationary communication satellites is approximately 30 MHz. A frequency allocation extending over multiple transponders is possible, however taking account of the reuse of existing hardware, the DPN TWSTFT frequency separation $2F_1$ was set to approximately 20 MHz. In following examples we set $2F_1 = 20.24$ MHz.

Once the frequency separation is fixed, the lower limit of the chip rate R_C for the pseudo random noise can be calculated from Equation (31). The time required for ambiguity determination was set to 1 second and the chip rate R_C to 100 kcps with some margin. The delay measurement precision σ_τ for this frequency allocation is expected to be 20 ps or less from Equation (30).

In practice, the transponder bandwidth was set to 200 kHz and the chip rate to 204.6 kcps in order to make the power density as flat as possible.

3.2 Generation of transmission signal

Usually, pseudo random noise (for binary phase shift keying BPSK) is generated using hardware by 180-degree carrier phase shift[3]. Similarly BOC is generated by shifting the phase of pseudo random noise using a higher frequency binary subcarrier[4]. This signal generation method is widely used since it can be realized with a simple circuit, however it cannot be flexibly modified because it is con-

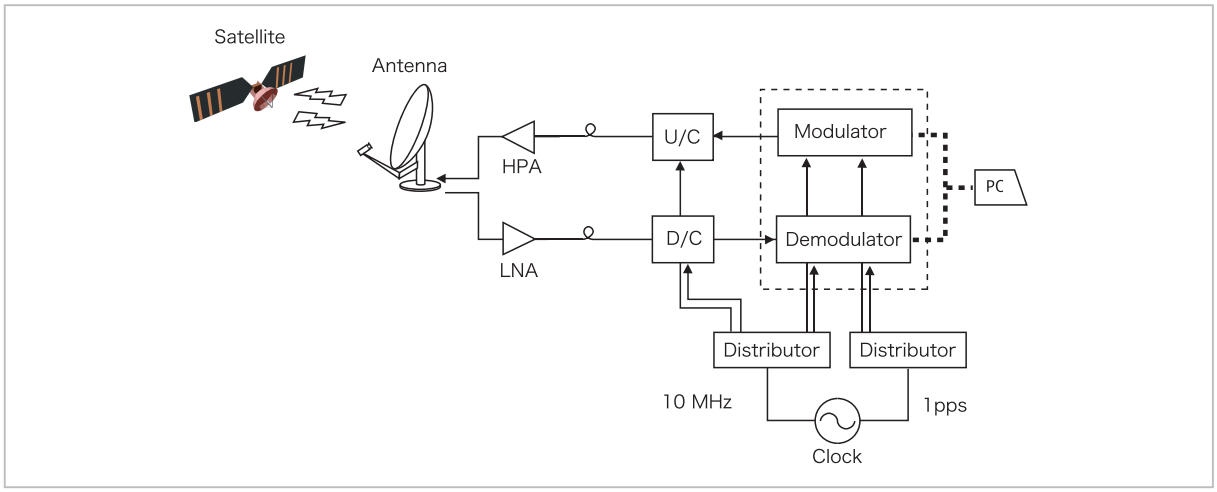

Fig.7 *Conventional TWSTFT system configuration*

Table 1 *Conventional TWSTFT system specifications*

Antenna	aperture diameter	1.8 m
	polarization	linear-polarization (orthogonal for transmission and receiving)
High power amplifier	maximum power	10 W
	operating power	2 W or less
	transmission frequency	13.75–14.5 GHz
Low noise amplifier	noise temperature	60 K or less
	receive frequency	10.9–12.75 GHz
Transmission frequency convertor	intermediate frequency	50–90 MHz
Receiving frequency convertor	intermediate frequency	50–90 MHz

structed from hardware. On the other hand, it is not always possible to acquire the frequency separation and bandwidth required for DPN TWSTFT on communication satellite transponder. Therefore we adopted direct IF signal generation using arbitrary waveform generator to realize flexible frequency allocation.

Another reason for adopting an arbitrary waveform generator is elimination of the instability of an analog circuit. Usually, out-of-band signals which are restricted by the radio regulations are rejected in IF frequency by applying high rejection performance filters such as SAW filters, however the group delay properties of these types of analog filters are easily affected by environmental temperature changes. We can avoid the instability of analog filters by adopting an arbitrary waveform generator which can generate waveforms ideally shaped in a computer using digital filters.

There are already a large number of high performance arbitrary waveform generators commercially available, however we have developed an arbitrary waveform generator which is low cost and dedicated to DPN TWSTFT with limited functions (Fig. 8). Table 2 shows the specifications of the arbitrary waveform generator we developed.

Fig.8 *DPN TWSTFT transmitter (left) and receiver (right)*

1,024,000 samples at a maximum are created on a computer and uploaded to the arbitrary waveform generator via USB. The arbitrary waveform generator periodically converts the received samples to 204,600,000 samples of analog signals every second, then outputs the analog signals synchronously with the external reference signal. Practically, we set period (code length) to 1,023,000 samples per 5 ms in order to complete a period every second on the second. In addition, in order to specify the code synchronized with external 1 pps signals, each code phase is changed (0 degrees or 180 degrees) according to overlay signals. We used a gold code used in GPS L1 C/A signals[10] for the pseudo random noise. A 204.6 kcps pseudo random noise was generated inside the computer, restricted to 100 kHz by a digital filter with 16385 taps and then converted to a higher frequency by multiplying 2 sine waves of 66.13 MHz and 86.13 MHz. Figures 9–11 show an example of a signal generated by the arbitrary waveform generator according to the waveform and the overlay signal generated as above.

These figures show the signal spectra which were generated by the arbitrary signal generator, converted to radio frequency, amplified by a high power amplifier and then acquired at the monitor port of the high power amplifier.

Some spurious signals can be seen in the generated signal. However, when carrying out TWSTFT using a usual diameter antenna, a

Table 2 *Specifications for arbitrary waveform generator*

Sample frequency	204.6 Msps
D/A bits	8 bits
No. of channels	2
External reference signal	10 MHz and a pulse signal per second (1 PPS)
memory for waveform data	512 kB/channel
memory for overlay data	64 kB/channel
data interface	USB 2.0

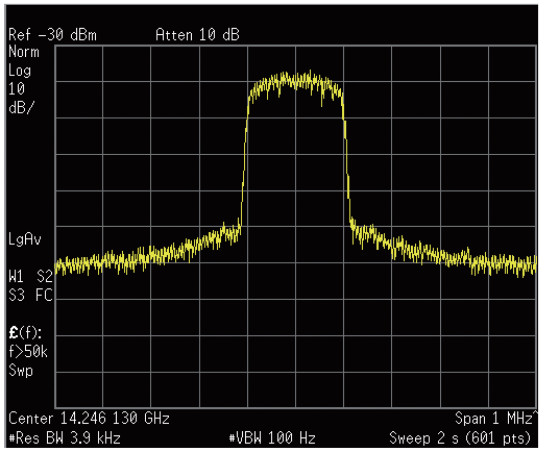

Fig.9 *DPN signal spectrum (lower frequency)*

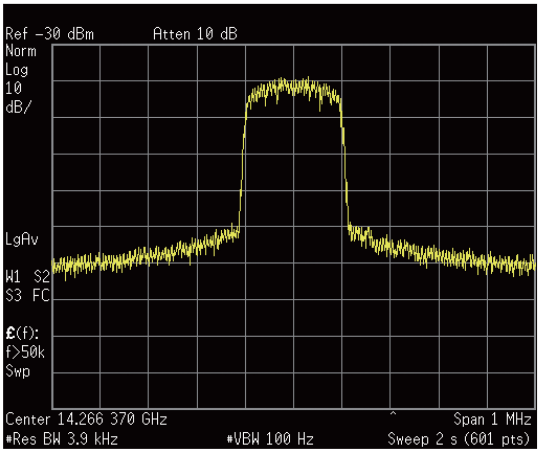

Fig.10 *DPN signal spectrum (higher frequency)*

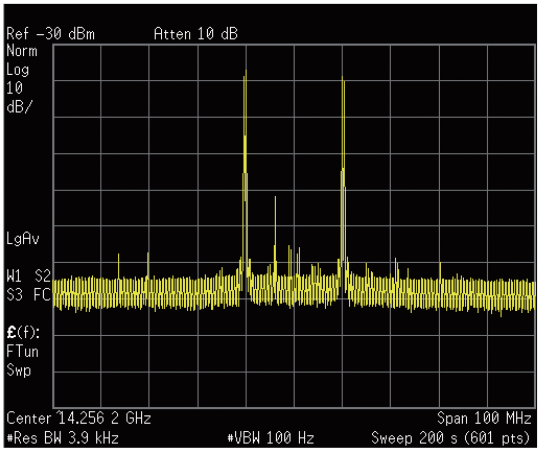

Fig.11 *DPN signal spectrum (entire signal)*

transmission power of 0.5 W (0.25 W pseudo random noise for each) or less is sufficient, so these spurious signals are sufficiently low enough to clear the Japanese radio regulations.

In addition, we can easily adjust the parameter for the digital filter in a computer to fit the frequency bandwidth of waveforms to licensed frequency bandwidth.

3.3 Signal processing for received data

The signal received by the antenna is amplified with a low noise amplifier and converted to the IF band signal as conventional TWSTFT. For processing of IF signals, a versatile AD converter[11][12] developed originally for VLBI was used. The specifications of the versatile AD converter are shown in Table 3.

Because the effective signal band for DPN is split into two 200 kHz bands, it is sufficient to sample data with a sample rate of 500 kHz using 2 channels of a versatile AD converter after being split into two signals and removing the undesired components using narrow band filters in the analog circuit, however in order to eliminate the instability of the analog circuit, we adopted a method to sample two bands together at 64 Msps (Fig. 12). The IF output frequency of usual frequency converters used in TWSTFT is 50–90 MHz, so after passing the IF signal through 64 MHz to 96 MHz band pass filters we sampled the data with the 64 Msps 8 bit under the sampling mode of the versatile AD converter. Two 2 MHz bands (2–4 MHz and 22–24 MHz) were extracted from the sampled signal by applying a 64 tap digital filter equipped in the versatile AD converter (Fig. 13). Signal stream after the filtering was then decimated to 1/8 to decrease data rate to 8 Msps (Fig. 14), and then output to a computer via a USB interface. We can significantly reduce the load of calculation on a computer by this decimation.

However, as can be seen from Fig. 13, because the number of taps of the digital filter was not enough, the noise from undesired frequency components was approximately -15 dB lower than the noise of the desired frequency band. This undesired noise acts as folding noise resulting from the decimation and causes the S/N degradation of approximately 10%,

Table 3 *Specifications of versatile AD convertor*

Sampling frequency	40 kHz–64 MHz, 11 modes
A/D bits	1, 2, 4, 8 bits
Number of channels	4
External reference signal	10 MHz and a pulse per second (1 PPS)
Interface	USB 2.0

however the group delay precision degradation resulting from this S/N degradation can be estimated from Equation (30) to be several percent. Because a larger scale FPGA is necessary to increase the number of taps of the digital filter equipped in the versatile AD convertor, considering cost effectiveness, we permit this degree of degradation.

For Figs. 12–14, in order to make the spectrum structure more visible, we set C/N_0 of the DPN signal rather high.

In the computer, digital filter processing at 200 kHz bandwidth, cross correlation with replica code, and the group delay and carrier phase determination are made sequentially and independently for each band, and finally fine group delay was determined by linking phases of two bands[13].

4 Conclusion

We have introduced the theoretical limits of delay measurement precision and realization methods for DPN TWSTFT, which is a new TWSTFT method. By using this method, we can improve the delay measurement precision by one order of magnitude. Since the occupied bandwidth of satellite transponders can be reduced greatly by introducing this method, we can cut down the operational cost by one order. Hereafter, we will continue verification experiments in international time comparisons aimed towards practical application.

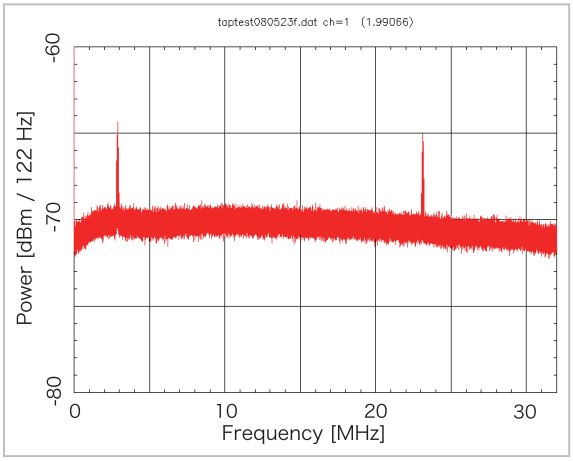

Fig.12 *DPN signal sampled at 64 Msps*

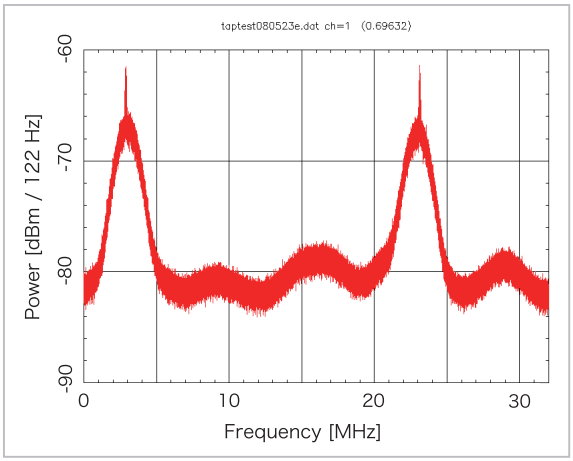

Fig.13 *DPN signal after filtering*

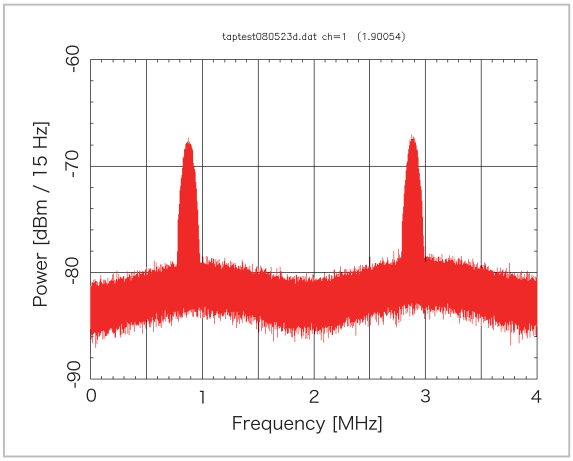

Fig.14 *DPN signal after decimation to 8 Msps*

References

1 D. Kirchner, “Two-Way Time Transfer Via Communication Satellite,” Proc. IEEE, pp. 983–990, 1979.

2 B. Fonville et al., “Development of Carrier-phase-based Two-way Satellite Time and Frequency Transfer (TWSTFT),” PTTI, pp. 149–164, 2004.

3 R. Peterson et al., “Introduction to Spread Spectrum Communications,” Prentice Hall, 1995.

4 J. W. Betz, “Binary Offset Carrier Modulations for Radio Navigation,” Journal of The Institute of Navigation, Vol. 48, No. 4, Winter 2001-2002.

5 W. Schafer, “New trends in two-way time and frequency transfer via satellite,” PTTI, 1999.

6 J. Amagai et al., “Current Status of Two-way Satellite Time and Frequency Transfer Using a Pair of Pseudo Random Noises,” ATF2008, pp. 267–271, 2008.

7 T. Gotoh et al., “Development of A GPU Based bTwo-way Time Transfer Modem,” CPEM, 2010.

8 A. R. Whitney, “Precision geodesy and astrometry via very-long-baseline interferometer,” Ph.D. Thesis, M. I. T., 1974.

9 F. Takahashi, T. Kondo, Y. Takahashi, “Very Long Baseline Interferometer,” Ohmsya, May 2000.

10 “IS-GPS-200D,” July, 2004.

11 M. Kimura et al., “The implementation of the PC based Giga bit VLBI system,” IVS CRL-TDC News, No. 21, pp. 31–33, 2002.

12 T. Kondo, Y. Koyama, R. Ichikawa, M. Sekido, E. Kawai, and M. Kimura, “Development of the K5/VSSP System,” J. Geodetic Soc. Japan, Vol. 54, No. 4, pp. 233–248, 2008.

13 A. E. E. Rogers et al., “Very long baseline interferometry with large effective bandwidth for phase-delay measurements,” Radio Science., 5, 10, Oct. 1970.

(Accepted Oct. 28, 2010)

AMAGAI Jun

Research Manager, Space-Time Standards Group, New Generation Network Research Center

Time and Frequency, Radio Interferometer

GOTOH Tadahiro

Senior Researcher, Information Governance Promotion Team, Information Management Office

Time and Frequency Standard